AGU PUBLICATIONS

Water Resources Research

RESEARCH ARTICLE
10.1002/2016WR019651

# Inferring hydraulic properties of alpine aquifers from the propagation of diurnal snowmelt signals

**Barret L. Kurylyk[1,2] and Masaki Hayashi[1]**

[1]Department of Geoscience, University of Calgary, Calgary, Alberta, Canada, [2]Now at School of Geography and Earth Sciences, McMaster University, Hamilton, Ontario, Canada

**Key Points:**
- Many alpine aquifers and streams are characterized by diurnal flow signals caused by snow or glacier melt
- Small shallow aquifers retain diurnal signals at their outlet but the signals are damped and lagged
- Results from a numerical groundwater model demonstrate that these signals can help characterize aquifer storage and hydraulic properties

**Correspondence to:**
B. Kurylyk,
barret.kurylyk@ucalgary.ca

**Citation:**
Kurylyk, B. L. and M. Hayashi (2017), Inferring hydraulic properties of alpine aquifers from the propagation of diurnal snowmelt signals, *Water Resour. Res.*, *53*, 4271–4285, doi:10.1002/2016WR019651.

Received 15 AUG 2016
Accepted 1 MAY 2017
Accepted article online 8 MAY 2017
Published online 25 MAY 2017

**Abstract** Alpine watersheds source major rivers throughout the world and supply essential water for irrigation, human consumption, and hydroelectricity. Coarse depositional units in alpine watersheds can store and transmit significant volumes of groundwater and thus augment stream discharge during the dry season. These environments are typically data scarce, which has limited the application of physically based models to investigate hydrologic sensitivity to environmental change. This study focuses on a coarse alpine talus unit within the Lake O'Hara watershed in the Canadian Rockies. We investigate processes controlling the hydrologic functioning of the talus unit using field observations and a numerical groundwater flow model driven with a distributed snowmelt model. The model hydraulic parameters are adjusted to investigate how these properties influence the propagation of snowmelt-induced diurnal signals. The model results expectedly demonstrate that diurnal signals at the talus outlet are progressively damped and lagged with lower hydraulic conductivity and higher specific yield. The simulations further indicate that the lag can be primarily controlled by a higher hydraulic conductivity upper layer, whereas the damping can be strongly influenced by a lower hydraulic conductivity layer along the base of the talus. The simulations specifically suggest that the talus slope can be represented as a two layer system with a high conductivity zone (0.02 m $s^{-1}$) overlying a 10 cm thick lower conductivity zone (0.002 m $s^{-1}$). This study demonstrates that diurnal signals can be used to elucidate the hydrologic functioning and hydraulic properties of shallow aquifers and thus aid in the parameterization of hydrological models.

## 1. Introduction

On a global scale, alpine watersheds provide critical water supply for human consumption, ecosystem functioning, irrigation, hydroelectricity, and other industrial activities [e.g., *Kaser et al.*, 2010; *Viviroli et al.*, 2007, 2011]. Mountain regions have experienced intensified warming compared to lowland regions [*Pepin et al.*, 2015], and these atmospheric changes are eliciting concern over the future state of alpine water resources and the impacts to downstream environments [*Brown et al.*, 2007; *Zierl and Hugmann*, 2005]. Physically based alpine hydrological models are useful tools for investigating the possibility of hydrologic regime shifts due to future climate warming and for informing best practices for water resources management in the context of an uncertain future. A number of recent studies have used numerical groundwater flow models [e.g., *Camporese et al.*, 2014; *Evans et al.*, 2015; *Lowry et al.*, 2010; *Markovich et al.*, 2016] or semidistributed hydrological models [e.g., *Fang et al.*, 2013; *Rasouli et al.*, 2014] to investigate the importance of surface and/or subsurface hydrological processes in mountainous environments. However, there is a paucity of hydrogeologic data in mountain regions [*Tague and Grant*, 2009], and thus properly parameterizing subsurface hydrological or hydrogeological models in alpine environments remains a persistent and important challenge.

One common approach for estimating storage and transmission properties of aquifers with no available direct subsurface data is through the analysis of base flow recession characteristics using approximate solutions to the *Boussinesq* [1877] equation [see *Brutsaert*, 2005; *Troch et al.*, 2013, for reviews]. Most standard recession approaches have been developed and applied for mildly sloping aquifers for which the slope is not an important driver for subsurface flow. However, empirical or semiempirical equation modifications have been proposed for steeply sloping aquifers such as those commonly observed in alpine environments

[e.g., *Rupp and Selker*, 2006a], and several studies have applied recession flow analysis techniques to estimate hydraulic properties of alpine aquifers [*Clow et al*., 2003; *Mendoza et al*., 2003; *Pauritsch et al*., 2015].

In most cases when recession flow analyses are applied, *persistent drainage* conditions are assumed as in the case of winter base flow when streamflow is predominantly sourced by groundwater discharge. The analysis of naturally occurring diurnal variations in stream or groundwater levels provides an opportunity for estimating aquifer hydraulic properties under *transient conditions* caused by cyclical loading. Diurnal signals in stream discharge and stage can be caused by a number of processes, including snowmelt [*Caine*, 1992; *Loheide and Lundquist*, 2009; *Mutzner et al*., 2015], glacier melt [*Condom et al*., 2013; *Crossman et al*., 2011], and evapotranspiration (ET) [*Bond et al*., 2002; *Deutscher et al*., 2016; *Graham et al*., 2013]. Several studies have analyzed the propagation of diurnal hydraulic pulses from a stream to a hillslope (or vice versa) to determine hydraulic conductivity using an analytical solution to a diffusion equation subject to a Fourier series boundary condition [e.g., *Loheide and Lundquist*, 2009; *Magnusson et al*., 2014]. The investigation of diurnal variations in groundwater levels or stream discharge is an emerging research field, and additional relevant discussions can be found in reviews by *Lundquist and Cayan* [2002] and *Gribovszki et al*. [2010].

With the exception of *Pauritsch et al.* [2015], previous studies have employed some variant of the analytical approaches previously mentioned to estimate hydraulic properties of steeply sloping aquifers from either diurnal signals or discharge recession characteristics. However, there are a number of difficulties inherent in these techniques. Most notably, analytical solutions to the *Boussinesq* [1877] equation are approximate due to its nonlinear form, and thus empirical calibration parameters (in addition to hydraulic parameters) can be required to characterize the response [*Brutsaert*, 1994]. Such solutions are often characterized by difficulty in curve fitting, including determining transition points [*Mendoza et al*., 2003] and appropriate time increments for analysis [*Rupp and Selker*, 2006b]. These analytical approaches also typically assume homogeneous hydraulic properties. Finally, the analytical solution to the diffusion equation subject to a Fourier series boundary condition invokes many assumptions including a horizontal aquifer base and aquifer stage fluctuations that are insignificant compared to aquifer thickness [*Magnusson et al*., 2014]. Both of these assumptions can be invalid in small alpine aquifers, which are often characterized by thin saturated zones and steep slopes.

The present study is focused on a small alpine talus slope in the Lake O'Hara watershed of the Canadian Rockies (section 2). The outlet spring from this talus exhibits diurnal discharge signals during the snowmelt period [*Muir et al*., 2011]. The overall goal of the present study is to demonstrate how a numerical groundwater flow model can be used to simulate the propagation of diurnal hydraulic pulses and thereby investigate the hydraulic properties and hydrologic functioning of alpine aquifers and aid in the parameterization of hydrological models in these environments. Specifically, the objectives of this study are (1) to apply a *Boussinesq* [1877] equation solver to model the talus discharge response to daily snowmelt recharge pulses simulated by a distributed snowmelt model, (2) to adjust the hydraulic and storage properties (i.e., specific yield, hydraulic conductivity of upper layer, and hydraulic conductivity of lower layer) of the groundwater model to investigate how these properties influence the signal propagation and to achieve general congruence between the simulated and observed lagging and damping of the output signals, and (3) to compare the numerical model results with those obtained using a simple analytical solution.

## 2. Study Site and Data Collection

### 2.1. Study Site

The talus slope investigated in this study is located in the Opabin subwatershed (51° 20′ 41″, 116° 19′ 32″) of the Lake O'Hara Watershed in Yoho National Park, British Columbia, Canada (Figure 1a, inset). The Opabin watershed is approximately 5 $km^2$ and ranges in elevation from about 2020 to 3500 m above sea level with a diverse land cover composed of bedrock (53%), moraine (17%), subalpine vegetation (14%), talus slopes (11%), glacier (4%), and lakes (1%) [*Hood and Hayashi*, 2015]. An automated weather station is located within the watershed to support a long-term study of alpine hydrological and hydrogeological processes [e.g., *Hood et al*., 2006; *McClymont et al*., 2010; *Langston et al*., 2011; *Muir et al*., 2011]. Mean monthly air temperature in the Opabin watershed ranges from −9.6°C (January) to 10.4°C (July), and mean annual precipitation is between 1000 and 1200 mm [*Hood and Hayashi*, 2015]. The majority of precipitation occurs as snow, and the Opabin watershed is snow-covered for up to 10 months of the year. The underlying and exposed bedrock is predominantly thickly bedded quartzite and quartzose sandstone with layers of Lower Cambrian

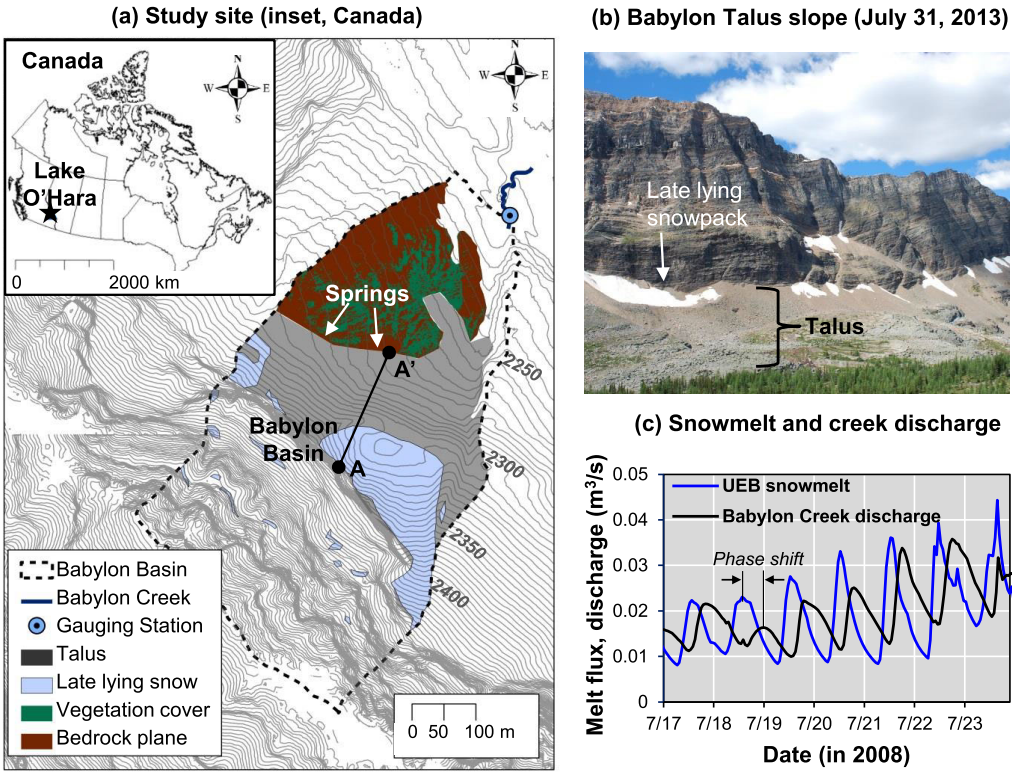


**Figure 1.** (a) Map of the Babylon talus basin in the Opabin subwatershed (snow distribution presented for 24 July 2008, modified from *Muir et al*. [2011]) of the Lake O'Hara Watershed in British Columba, Canada (inset), (b) photograph of the talus slope (photo credit: Andrius Paznekas), and (c) Plot of measured discharge in Babylon Creek (black) and the snowmelt (blue) simulated in the Utah Energy Balance model (section 3.2).

Gog Group shale, siltstone, and sandstone [*Desjardins et al*., 2010; *Lickorish and Simony*, 1995]. The talus units in the Opabin subwatershed are primarily cobble and boulder sized materials derived from quartzite intermingled with fine to coarse-grained matrix sediments [*Muir et al*., 2011].

This study focuses on the Babylon talus and its associated subwatershed, which is located along the southwest border of the Opabin watershed (Figure 1a). Electrical resistivity tomography (ERT) and ground penetrating radar (GPR) surveys of the Bablyon talus indicated that the talus material is less than 15 m thick and is mostly dry except in the saturated zone at the base [*Muir et al*., 2011]. The "Babylon basin" is approximately $2.8 \times 10^5$ m$^2$ in surface area and is drained by Babylon Creek which exits the northeast corner of the basin (Figure 1a). The Babylon talus sources two small springs located at the base of the talus slope (Figure 1a), and discharge from these springs flows to Babylon Creek along the surface of the bedrock plane. *Muir et al*. [2011] used the standard kinematic-wave equation [*Bedient and Huber*, 2002] to demonstrate that the surface travel time along the bedrock plane from the springs to the gauging station is minimal (<1 h), and thus it is not considered in the present study. During the summer months, the melting of late lying snow (Figure 1b) provides the primary hydrologic input to the talus causing the discharge from the springs and the stage in Babylon Creek to exhibit diurnal fluctuations (see the black line in Figure 1c, extracted from *Muir et al*. [2011]). During the period shown in Figure 1c, evapotranspiration flux from the bedrock plane ($5.2 \times 10^4$ m$^2$), measured with an eddy-covariance system, was on the order of 1.3 mm d$^{-1}$, resulting in a total volumetric loss rate of $8 \times 10^{-4}$ m$^3$ s$^{-1}$ over the bedrock plane. This is much smaller than the creek discharge rate, and hence, the diurnal cycle of evapotranspiration is expected to have little control on diurnal discharge fluctuations.

### 2.2. Hydrologic Data Collection

Hydrologic data were collected as previously described by *Muir et al*. [2011]. Discharge at the gauging station in Babylon Creek (Figure 1a) was estimated from the area velocity method with weekly velocity measurements taken with a hand-held propeller flow meter (Global Water, FP101). Continuous (every 10 min)

stage recording was conducted with pressure transducers (In-Situ Inc., Aqua Troll 200) installed in a stilling well, and discharge was estimated from the water stage using the stage-discharge rating curve developed from manual measurements. In addition to precipitation measurements recorded at the nearby (300 m southeast) automated weather station, precipitation was also monitored on the talus using a tipping-bucket rain gauge (Onset, RG3-M). Only trace amounts ($<1$ mm $d^{-1}$) of precipitation occurred during the period for which groundwater flow simulations were performed in this study (17–23 July 2008), and thus snowmelt was considered to be the only hydrologic input to the talus. The timing and spatial extent of snow cover was monitored using oblique-angle terrestrial photographs as detailed in *Hood and Hayashi* [2015].

## 3. Modeling Approach

### 3.1. Overall Modeling Approach

The propagation of the diurnal snowmelt signals was simulated using a sequential modeling approach as indicated in Figure 2a. First, a snowmelt model (section 3.2) was used to generate the snowmelt infiltration. This flux then became the upper boundary condition for the saturated groundwater flow model. These models were explicitly linked via this one-way coupling rather than implicitly coupled. The groundwater table is approximately 10 m below the ground surface, and the coarse boulders in the unsaturated zone allow for rapid vertical preferential flow toward the water table [*Muir et al.*, 2011]. Variations in the groundwater table elevation and unsaturated zone moisture content would not greatly influence snowmelt infiltration dynamics, and thus implicitly coupling these models is not necessary for these field conditions. Note that the residence time and signal modulation in the unsaturated zone were not considered (see Limitations) as snowmelt infiltration was assumed to instantaneously recharge the aquifer via rapid preferential flow [*Muir et al.*, 2011]. Residence time and signal modulation in the saturated zone is postulated to be higher due to the lower hydraulic gradients and the much greater lateral distance ($\sim$200 m) than vertical distance ($\sim$10 m unsaturated zone).

### 3.2. Snowmelt Model: Utah Energy Balance Model

The snowmelt flux is difficult to measure directly on the steep talus slope, and thus it was simulated using the Utah Energy Balance (UEB) model [*Tarboton et al.*, 1995; *Tarboton and Luce*, 1996]. *Hood and Hayashi* [2015] set up the UEB model on each of the 7780 grid cells (25 m by 25 m) covering the Opabin watershed and conducted model calibration and validation using biweekly measurements of snow water equivalent at 10 snow courses distributed over the watershed. The snowmelt output data from their UEB model ran for 2008 were extracted for all grid cells within the Babylon basin to calculate total snowmelt flux leaving the bottom of the snowpack and entering the talus unit as presented in Figure 1c (blue line). The snowmelt flux was applied as the boundary condition to drive simulations of subsurface flow in the numerical

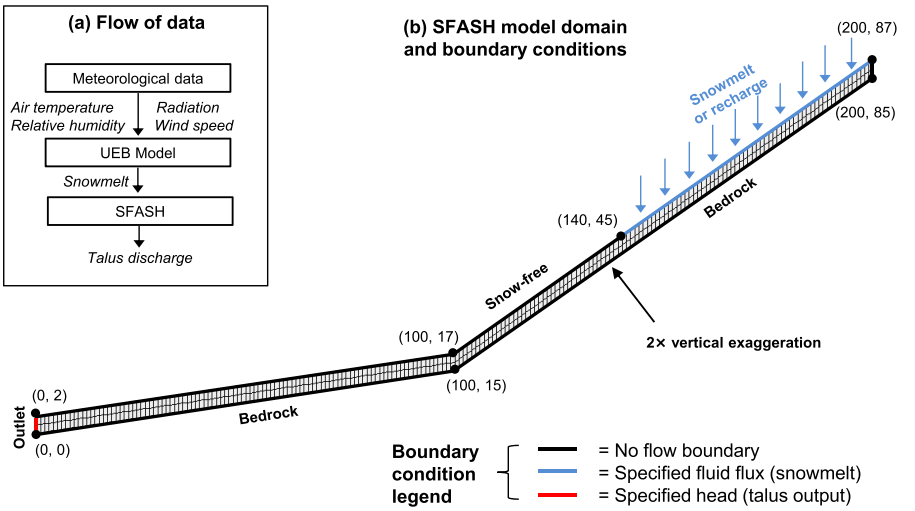


**Figure 2. (a)** Flow of data through the modeling sequence and (b) modeling domain and boundary conditions for the SFASH simulations. The *x* and *y* coordinates (in meters) of each vertex in the model outline are noted.

groundwater model of the Babylon talus. Note that the UEB model considers the transit time in the snowpack, and thus the flux presented in Figure 1c is the simulated timing of the infiltration flux.

A spatially variable snowmelt model was employed despite the small domain because snowmelt contributing areas can change due to variation in snowmelt rates [*Marsh and Pomeroy*, 1996; *DeBeer and Pomeroy*, 2010]. Variations in the surface energy balance and snowmelt rates are often apparent in alpine watersheds with complex terrain [*Marks and Dozier*, 1992; *Marks et al*., 1999]. The snowmelt flux (mm $d^{-1}$) applied as input to the SFASH model (section 3.3) was the UEB-simulated hourly snowmelt flux spatially averaged across the snow-covered portion of the talus. Only matrix meltwater flow was considered in the UEB model simulations, but preferential meltwater flow [*Marsh and Woo*, 1984], which is especially characteristic of cold snowpacks, can be a source of errors in hydrology and energy balance calculations [e.g., *Pomeroy et al*., 1998]. However, preferential flow through the snowpack is not expected to be important during the period of the present study as the snowpack was mature and isothermal.

### 3.3. Saturated Groundwater Flow Model: SFASH

#### 3.3.1. SFASH Overview

The **S**imple **F**ill **A**nd **S**pill **H**ydrology (SFASH) model [see *Wright et al*., 2009 for details] was selected to simulate the lateral transmission of the hydraulic pulses through the saturated zone. SFASH was developed as a computationally efficient tool to examine groundwater flow through hydraulically conductive materials overlying a surface with complex topography. It simulates the filling and spilling of subsurface depressions [e.g., *Spence and Woo*, 2003; *Tromp-van Meerveld and McDonnell*, 2006] by solving a two-dimensional groundwater flow equation (see below). Originally used to simulate groundwater flow through highly porous peat overlying ice-rich permafrost, the model is suitable for any environments characterized by permeable sediments (e.g., talus) overlying impermeable material. SFASH solves the Boussinesq equation rather than the more rigorous three-dimensional Richards equation, but *Steenhuis et al*. [1999] and *Paniconi et al*. [2003] have shown that variations of these two distinct formulations produce similar outflow hydrographs for most conditions. Specifically, SFASH solves the two-dimensional Boussinesq equation [e.g., *Wigmosta and Lettenmaier*, 1999]:

$$\frac{\partial}{\partial x}\left(T_x\frac{\partial h}{\partial x}\right)+\frac{\partial}{\partial y}\left(T_y\frac{\partial h}{\partial y}\right)=S_y\frac{\partial h}{\partial t}-R \tag{1}$$

where $h$ is the hydraulic head (m), $x$ and $y$ are the distances in the two ordinate directions (m), $T_i$ is the transmissivity in direction $i$ ($m^2$ $s^{-1}$), $S_y$ is the specific yield, $t$ is time (s), and $R$ is the recharge rate (m $s^{-1}$). This formulation assumes that there is no vertical hydraulic gradient and that the horizontal hydraulic gradient is equivalent to the water table slope. SFASH solves equation (1), which is nonlinear due to the dependence of transmissivity on hydraulic head [e.g., *Bishop et al*., 2011], using the implicit finite difference approach with a modified Picard scheme [*Celia et al*., 1990, equation (16)]. Only the one-dimensional version of equation (1) was solved in SFASH in this study.

#### 3.3.2. SFASH Domain and Boundary and Initial Conditions

Figure 2b presents the model domain and boundary conditions used in the SFASH simulations. The geometry of the model domain was estimated from a digital elevation model as well as geophysical surveys conducted by *Muir et al*. [2011]. The domain was represented as a two-dimensional slice through the talus slope along transect A-A′ (Figure 1a). The location of the snowmelt input was estimated from the oblique-angle terrestrial photographs [*Hood and Hayashi*, 2015]. This SFASH boundary (blue line, Figure 2b) was assigned a specified flux equal to the hourly snowmelt flux simulated in the UEB model averaged over the entire snow-covered portion of the Babylon subbasin (Figure 1a) to account for variations in the surface energy balance as well as the distribution of snow cover. All other boundaries were no-flow boundaries except for the discharge point at the toe of the talus (left side, Figure 2b), which was assigned a constant head boundary (0.02 m) based on the estimated thickness of the saturated layer [*Muir et al*., 2011]. The SFASH model domain height was chosen as 2 m (Figure 2b). Note that this does not imply that the depth to bedrock was a constant 2 m across the talus unit. Rather, since SFASH only simulates saturated zone dynamics, this depth was chosen because the thickness of the saturated domain never exceeded this value throughout the domain for all simulations. SFASH uses the actual simulated aquifer thickness, which must be less than the model domain height, to calculate the transmissivity (equation (3)) and consequent groundwater flow rates.

Initial conditions were generated by initiating an SFASH simulation with a uniform hydraulic head of 0.2 m throughout the domain and then running the simulation forward for a 72 h spin-up period. The first 24 h of spin-up time was a constant flux, and the following 48 h were the first two diurnal cycles (17–18 July 2008). Thus, eight days of simulated snowmelt fluxes (one day of constant flux and then diurnal signals from 17 to 23 July 2008, Figure 1c) were applied to drive the SFASH simulations, but only the last 5 days of SFASH simulations (19–23 July 19) were analyzed to determine the associated damping and lagging of the snowmelt input signals. The finite difference cells were 1 m by 1 m, and time steps began as 0.1 s and were allowed to vary to maximize computations efficiency. This spatiotemporal discretization was shown to achieve convergence despite the nonlinear nature of the governing equation and the rapidly varying specified flux boundary condition.

#### 3.3.3. SFASH Parameterization

To account for the effects of transmissivity feedback [e.g., *Bishop et al*., 2011], SFASH uses depth-varying saturated hydraulic conductivity set by a user-specified equation. The hydraulic conductivity equation used in this study is:

$$\log K(z) = \log K_B + (\log K_T - \log K_B)/[1 + (z/z_t)^n] \tag{2}$$

where $K(z)$ is the saturated hydraulic conductivity (m $s^{-1}$) at depth $z$ (m), $K_T$ and $K_B$ are, respectively, the saturated hydraulic conductivities at the top and bottom of the soil profile, $z_t$ is the transition depth (m) and $n$ is a dimensionless constant that controls the nature of the transition between $K_T$ and $K_B$. This conductivity profile was originally developed to present the power decrease in conductivity that is often observed in organic soils [*Quinton et al*., 2008]. However, the mathematical nature of this function also facilitates the development of a saturated hydraulic conductivity profile with a sharp transition between layers (Figure 3). Thus equation (2) was parameterized to represent a distinct two-layer system to account for the influence of a layer of fine materials at the base of the talus as postulated by *Davinroy* [2000] and further demonstrated by *Muir et al*. [2011] via geophysics. SFASH calculates the depth-integrated transmissivity based on the saturated hydraulic conductivity distribution (equation (2)), the depth to the water table ($z_w$, m) and the depth to the bedrock ($z_b$, m). In this study, $z_b$ was always 2 m as indicated in Figure 2b.

$$T = \int_{z_w}^{z_b} K(z)dz \tag{3}$$

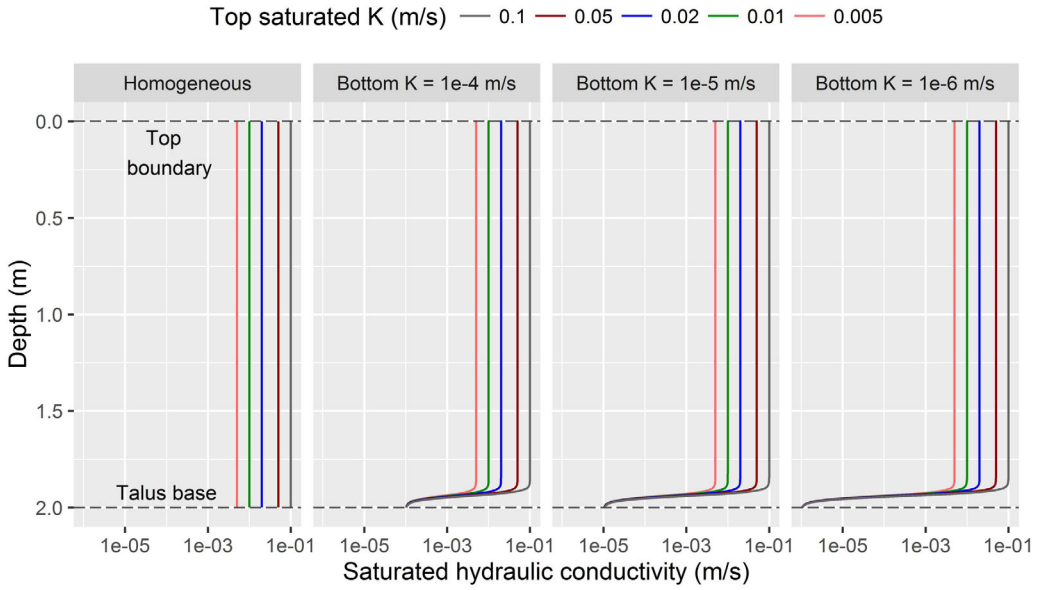


**Figure 3.** Hydraulic conductivity scenarios (depth below ground surface versus hydraulic conductivity) considered in the SFASH runs. The sloping base of the talus (bottom SFASH boundary) is always 2 m below the sloping top boundary of the SFASH domain as noted by the horizontal dashed lines at depths of 0 and 2 m (see Figure 2b).

**Table 1.** SFASH Hydraulic Conductivity Settings Used in the 60 Model Runs[a]

| Conductivity Distribution | Top $K$ ($K_T$, m s$^{-1}$) | Bottom $K$ ($K_B$, m s$^{-1}$) | Specific Yield ($S_y$) | Equation (2) Constant, $n$ | Transition Depth ($z_t$, m) |
|---|---|---|---|---|---|
| Homogeneous | 0.005, 0.01, 0.02, 0.05, 0.1 | | 0.25, 0.3, 0.35 | | |
| 10 cm thick low K layer | 0.005, 0.01, 0.02, 0.05, 0.1 | 0.0001, 0.00001, 0.000001 | 0.25, 0.3, 0.35 | 175 | 1.94 |

[a]Equation parameters are from equation (2). See section 3.3.3 and Figure 3 for more details.

In total, 60 different combinations of $K$ distribution and specific yield were considered in the first part of this study. Fifteen homogeneous scenarios were selected, and these varied based on the specific yield (0.25, 0.3, and 0.35) as well as the uniform $K$ (0.005, 0.01, 0.02, 0.05, and 0.1 m s$^{-1}$). These values span the range of the bulk $K$ estimated by *Muir et al*. [2011] for the Babylon talus. Also, 45 additional model runs were conducted with an approximately 10 cm thick low $K$ zone at the base of the talus. These differed based on the top $K$, bottom $K$, and specific yield. Figure 3 visually presents the 20 $K$ distributions considered in this study; SFASH runs were performed for each of these $K$ distributions with three alternate values of specific yield (0.25, 0.3, 0.35), which represents the typical range for coarse-grained material [e.g., *Fetter*, 2001, p. 79]. Different $K_B$ values were assigned to investigate how the ratio of $K_T$ to $K_B$ influences damping and lagging. Note that 2 m depth in Figure 3 is the elevation of the bottom of the talus slope (bedrock surface) in the SFASH domain. Table 1 presents the equation (2) parameters used to generate the $K$ distributions in Figure 3.

#### 3.3.4. Model Postprocessing

The lag times between the diurnal snowmelt signals (SFASH input) and the subsequent measured and simulated diurnal discharge fluctuations were obtained using the cross-correlation function in R [*R Core Team*, 2014]. The daily damping factors between the input and output signals were calculated as:

$$Damping_j = 1 - \left( \frac{Max_O - Min_O}{Max_I - Min_I} \right)_j \tag{4}$$

where $Max_I$ and $Min_I$ are the maxima and minima of the daily input signals, $Max_o$ and $Min_o$ are the maxima and minima of the daily output signals, and $j$ indicates the day under consideration. A damping factor of 1 produced by equation (4) indicates that the signal is fully damped, whereas a damping factor of 0 indicates no damping. To calculate the damping factor for the field data, the simulated snowmelt flux was summed across the entire talus area so that the input signal was in the same units (m$^3$ s$^{-1}$) as the measured stream discharge signal (Figure 1c), and equation (4) could then be applied directly. For the SFASH simulations, both the input and output signals were in units of m$^3$ d$^{-1}$ m$^{-1}$ as only a unit aquifer width was considered. The cross-correlation analysis and damping factors calculations were only performed on the last five days of the SFASH simulations (19–23 July 2008), as the earlier data represented "spin-up" days for the model.

### 3.4. Analytical Solution

*Brutsaert* [2005, p. 415] presents an analytical solution to the linearized Boussinesq equation for hillslope drainage when the subsurface flow is primarily driven by gravity. This equation can be rearranged to isolate for the lag:

$$\tau = \frac{BS_y}{\sin(\gamma)\, K} \tag{5}$$

where $\tau$ is the lag between peak snowmelt and the spring discharge (s), $B$ is the length of the hillslope or aquifer (m), and $\gamma$ is the angle of the slope. Herein, $B$ is taken as the horizontal distance from the talus outlet to the center of the recharge boundary condition (170 m, Figure 2b), and $\gamma$ is taken as the slope of the lower portion of the talus (i.e., 15/100, Figure 2b).

## 4. Results and Discussion

### 4.1. Field Data Results

The cross-correlation analysis indicated that the maximum correlation between the snowmelt and the observed discharge signals (Figure 1c) was found with a lag of 7 h. The daily damping factors for the talus input and output signals calculated with equation (4) ranged from 0.24 to 0.51, and were on average 0.39 for the period (19–23 July 2008) for which SFASH simulations were performed for comparison. Note that

the daily mean total snowmelt simulated across the Babylon talus is similar in magnitude to the daily mean discharge in Babylon Creek (Figure 1c), which provides further evidence that it is the snowmelt fluxes which are providing the source water and driving the diurnal fluctuations in the creek discharge.

### 4.2. General Trends of Simulated Discharge Signals

Figure 4 shows the hourly snowmelt and SFASH-simulated talus discharge for the model runs. Results are presented for the homogeneous case as well as the three heterogeneous cases with the $K$ of the bottom layer ($K_B$) ranging from $1 \times 10^{-4}$ m s$^{-1}$ to $1 \times 10^{-6}$ m s$^{-1}$, as the layer of fines underlying the coarse cobbles and boulders is expected to be characterized by a significant reduction in $K$. A cursory analysis of the homogeneous runs (Figure 4a) indicates that the lagging and damping increase with decreasing $K$. Figure 4 only presents results for a specific yield ($S_y$) of 0.3, but the SFASH simulations conducted with other $S_y$ values indicated that the lagging and damping also increased with increasing $S_y$. Thus, as expected, both the lagging and damping are inversely related to the aquifer hydraulic diffusivity ($T/S_y$). Also, the homogeneous results indicate that the discharge signal is not significantly damped even when the lag approaches that observed in the field (e.g., $K_T = 0.01$ m s$^{-1}$, Figure 4a). This is in contrast with the field observations (Figure 1c) and provides the impetus for considering a thin low $K$ zone at the base of the talus, which could alter the interplay between the lagging and damping of the output signals. For example, the low $K$ zone should theoretically provide a low enough transmissivity when the groundwater table is lowered to allow for sustained discharge during the night.

Figures 4b–4d present the results when the thin lower $K$ zone was included at the bottom of the SFASH domain. The relationship between $K_B$ and the signal damping may seem counterintuitive at first. When $K_B$ is higher (i.e., $K_T/K_B$ is closer to 1, Figure 4b), the signal is more damped than when $K_B$ is lower as indicated by a comparison of Figure 4b with Figure 4c or 4d. This phenomenon is due to the influence of the layering on

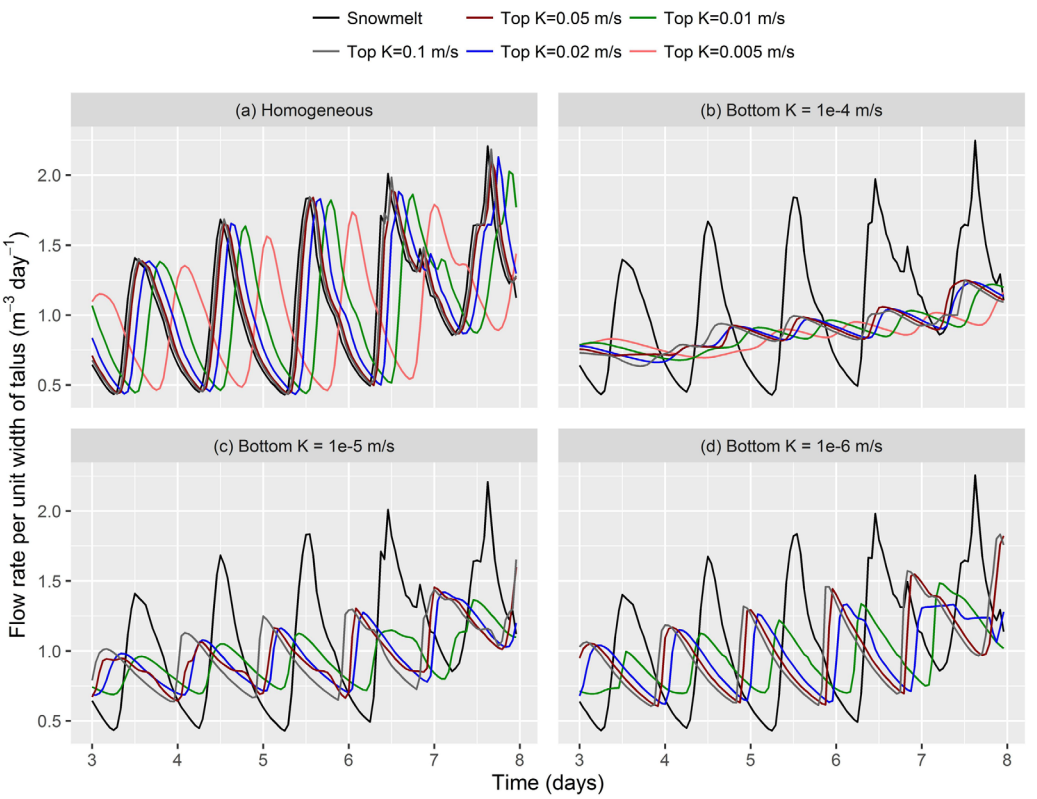


**Figure 4.** Inflows (snowmelt) and outflows (talus spring discharge) simulated in SFASH for each of the four $K_T$ values (colors) for (a) homogeneous conditions and for (b–d) a 10 cm thick low $K$ zone. Results are only presented for $S_y = 0.3$. Day 3 on the $x$ axis represents 19 July 2008. Colors in Figure 4 correspond to colors in Figure 3. Note that the $K_T = 0.005$ m s$^{-1}$ results are not presented for the heterogeneous cases as, in many cases, the output signals were too damped or lagged to accurately perform the cross-correlation or damping calculations.

the depth-integrated transmissivity (equation (3)), or more precisely to the transmissivity feedback effect [*Bishop et al.*, 2011]. The transmissivity is very sensitive to the thickness of the saturated aquifer and how that thickness is partitioned between the high and low $K$ zones. When $K_B$ is several orders of magnitude lower than $K_T$ (Figure 4d), the bottom layer contributes very little to flow, and the bulk system is more controlled by $K_T$. However, when $K_B$ begins to approach $K_T$ (Figure 4b), the bottom layer contributes more to the depth-integrated transmissivity and thus exerts more control on the flow dynamics. As expected, when the low $K$ zone is included at the base of the talus, the minima of the discharge signals are higher due to the sustained outflow during the night caused by the lower transmissivity (compare Figure 4a to 4b–4d). Figure 4 only qualitatively presents the damping and lagging of the diurnal signals; the following two sections will quantitatively consider the signal alterations by focusing on the calculated lags and damping factors.

### 4.3. Simulated Lags

Figures 5a–5d (top plots) presents the lags obtained from the cross-correlation analyses for each of the SFASH runs. For the homogeneous case, the lags are inversely related to $K$ as predicted by the analytical solution (equation (5)). For a given $K$ scenario, the lags increase with increasing $S_y$ (compare black and blue lines in Figure 5a), but the results for differing $S_y$ values converge at the higher $K_T$ values. For example for the homogeneous case, the difference in the calculated lags for the $Sy = 0.25$ and $Sy = 0.35$ runs was 5 h for $K$ =0.005 m s$^{-1}$ but 0 h when $K$ was increased to 0.1 m s$^{-1}$ (Figure 5a). The range of lags found for the homogeneous simulations (1–15 h) includes the lag observed in the field data (7 h). In general, Figure 5a

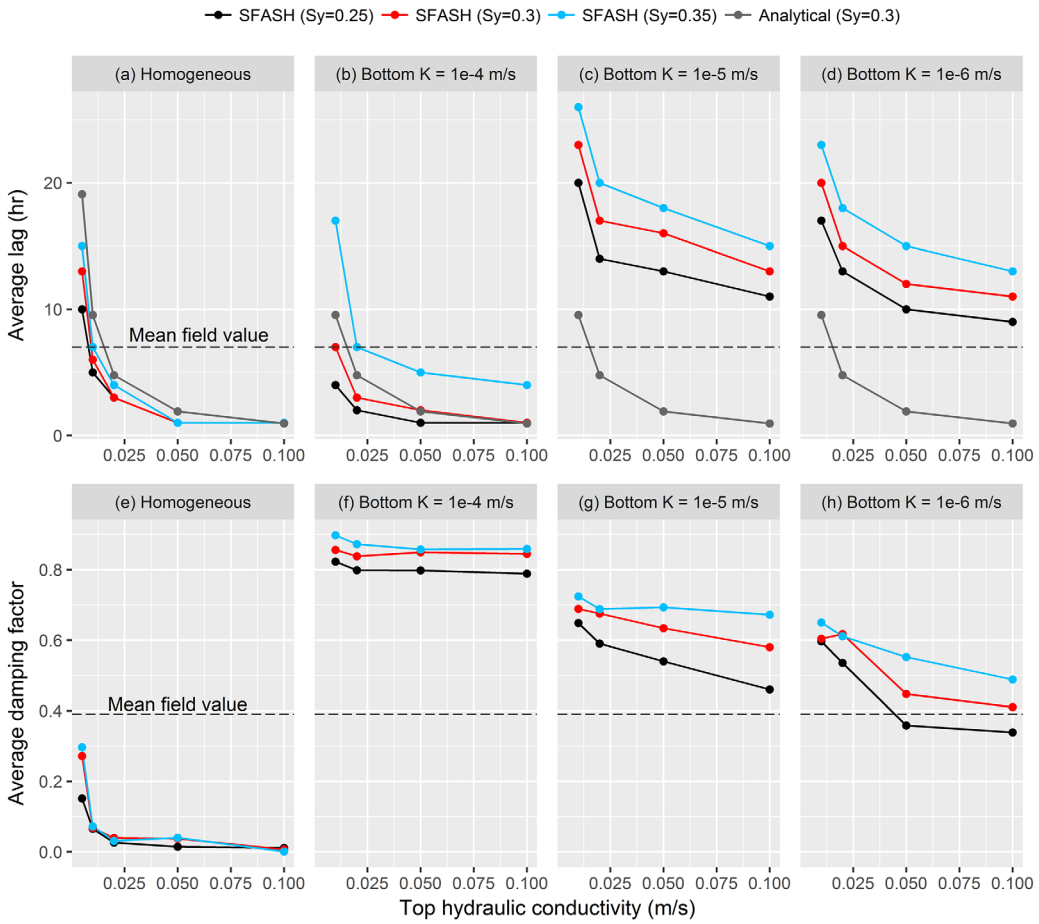


**Figure 5.** (top: a–d) Average lag between the diurnal snowmelt signal and the talus discharge versus $K_T$ for each SFASH runs. The analytical results (grey) were calculated with $S_y = 0.3$ (equation (3)); note that $K_T$ was used for the $K$ value in the analytical solution. (bottom: e–h) Average damping factors (equation (4)) versus $K_T$ for each SFASH run. The $K_T = 0.005$ m s$^{-1}$ results are not presented for the heterogeneous cases as, in many cases, the output signals were too damped or lagged to accurately perform the cross-correlation or damping calculations.

suggests a $K$ on the order of 0.01 m $s^{-1}$ for the homogeneous scenarios to achieve congruence between the simulated and measured lags. When the low $K$ zone is included with $K_B = 1 \times 10^{-5}$ m $s^{-1}$ or $1 \times 10^{-6}$ (Figures 5c and 5d), the simulated lags increase due to the reduction in the depth-integrated transmissivity. However, the lags are remarkably similar between these two figure plots, suggesting that the output signals are synchronous and that the lags are relatively insensitive to $K_B$ values below $1 \times 10^{-5}$ m $s^{-1}$, at least for the range considered in this study. The simulated lags for these two heterogeneous cases are all consistently higher than the lag obtained from the field data and indicated by the dashed line in Figure 5. In contrast, when $K_B = 1 \times 10^{-4}$ m $s^{-1}$ (Figure 4b), the simulated lags are much closer to those found for the homogeneous case, which suggests that, in this case, the conductivity of the upper layer $K_T$ is strongly influencing the lag dynamics.

The lags calculated with the analytical solution (equation (5)) are indicated by the grey line in Figures 5a–5d. The analytical results are consistent among all top figure plots since the solution cannot account for heterogeneities. If the analytical solution appropriately reproduces the numerical model physics, the red and grey series should overlap since these both represent the results for the same $S_y$. For the homogeneous scenario, the lags simulated in SFASH are similar but lower than those calculated with the analytical solution (Figure 5a). This implies that the $K$ inferred from the analytical solution lag would generally be too high for the homogeneous case. Presumably this difference is caused by the fact that SFASH considers the diffusive flow, whereas the analytical solution only considers gravity-driven flow. Since *Muir et al*. [2011] used the analytical solution to estimate $K$, the $K$ inferred from the SFASH simulations for the homogeneous case (0.01 m $s^{-1}$) is at the lower end of the range of $K$ values (0.01–0.03 m $s^{-1}$) estimated by *Muir et al*. [2011] for the same talus. For the heterogeneous runs represented in Figures 5c and 5d, the lags simulated in SFASH are higher than those obtained from the analytical solution since the latter does not account for the influence of the thin low $K$ zone. However, since the lag results for $K_B = 1 \times 10^{-4}$ m $s^{-1}$ (Figure 5b) are almost identical to those from the SFASH homogeneous runs, the analytical and simulated lags are also similar.

### 4.4. Simulated Damping Factors

Figures 5e–5h present the average damping factor for each SFASH run. These were found by first calculating the daily damping factors via equation (4), and then averaging the results for the last 5 days of simulation (19–23 July 2008). For the homogeneous case, the damping factors decrease with increasing $K$ and decreasing $S_y$. Unlike in the case of the lag results (Figure 5a), the range of damping factors calculated for the homogeneous runs (0.001–0.3, Figure 5e) does not include the average damping factor (0.39) calculated from the simulated snowmelt and measured discharge. This highlights the importance of considering both the damping factor and the lag when using diurnal signals to characterize the hydraulic properties of aquifers or hillslopes. The damping factors calculated from the simulations increase considerably when the low $K$ zone is included (Figure 5f–5h). Furthermore, the damping factor is sensitive to the exact value assigned to $K_B$, as the damping factors are much lower in Figure 5f than in Figure 5g or 5h for a given $K_T$ and $S_y$. The damping factors counterintuitively decreased as $K_B$ was reduced from $1 \times 10^{-4}$ m $s^{-1}$ (Figure 5f) to $1 \times 10^{-6}$ m $s^{-1}$ (Figure 5h), which suggests that the control of the lower conductivity layer on the damping dynamics depends on the ratio of $K_T$ to $K_B$. A very low $K_B$ value forces water to be routed through the high $K$ zone and thus increases the bulk aquifer transmissivity and decreases the damping factor. In general, the damping factors were more sensitive to $K_B$ than to $K_T$. This sensitivity contrasts with the simulated lags, which proved to be relatively insensitive to $K_B$ at the lower end, but very sensitive to $K_T$ (Figures 5c and 5d). These results suggest that, in a heterogeneous scenario with a high $K$ layer overlying a thin low $K$ zone, the lag of the diurnal signal is more controlled by $K_T$, while the damping is primarily controlled by $K_B$.

### 4.5. Qualitative Match Between Field and Simulated Data

The homogeneous SFASH simulations presented in Figures 4a, 5a, and 5e generally differ considerably from the field data with respect to the lag and/or the damping factor. For example, for $K = 0.01$ m $s^{-1}$ and $S_y = 0.35$, the simulated lag matches the observed lag (7 h, blue series, Figure 5a), but the simulated damping factor (0.07) is much lower than that of the field data (0.39). Thus, the $K$ inferred from just the signal lag would be always much higher than that inferred from the damping factor for the homogeneous scenarios. However, the fit between the simulations and field observations improves when the thin low $K$ zone is included, at least when the average lag and damping factors are considered. For example, the simulation performed with $K_T = 0.1$ m $s^{-1}$, $K_B = 1 \times 10^{-6}$ m $s^{-1}$, and $S_y = 0.25$ (black series, Figures 5d and 5h), has a

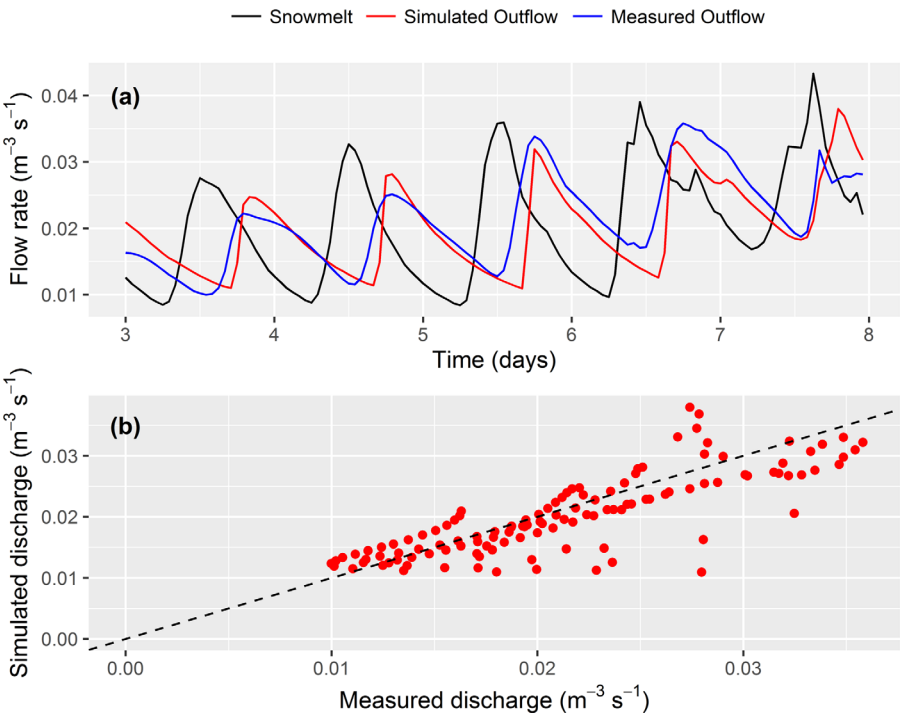


**Figure 6.** (a) Snowmelt, measured discharge, and simulated discharge versus model time for a simulation performed with $K_T = 0.02$ m s$^{-1}$, $K_B = 0.002$ m s$^{-1}$, and $S_y = 0.30$. In order to plot the measured (total flow) and simulated (flow per unit aquifer width) discharge values on the same axis, the simulated discharge values were scaled by the ratio of the total snowmelt across the basin area to the snowmelt inputted to the SFASH model. (b) Simulated hourly discharge versus measured hourly discharge for 19–23 July 2008.

damping factor (0.34) that is close to that calculated for the field data, and a lag of 9 h, which is slightly higher than that observed in the field.

Additional SFASH simulations were specifically performed to achieve general congruence between the simulated and observed damping and lagging of the snowmelt signal by manually adjusting the hydraulic parameters in SFASH. To obtain a quantitative measure of the goodness-of-fit, the *Nash and Sutcliffe* [1970] efficiency (NSE) values were calculated using the hydroGOF package in R. The fitting process was initiated using $K_T = 0.02$ m s$^{-1}$ as this $K$ value was estimated from tracer test results from the study site [*Muir et al.*, 2011]. The $K_B$ value was then gradually reduced until the average damping factor approached that observed in the field data. Figure 6 presents the measured data and the simulated results for a reasonable fit (NSE = 0.57, lag = 7 h, damping factor = 0.46) obtained from this manual calibration procedure with $K_T = 0.02$ m s$^{-1}$, $K_B = 0.002$ m s$^{-1}$, and $S_y = 0.30$. Higher NSE values could be obtained, but the resultant output signals became increasingly underdamped in comparison to the measured discharge. In general, the signal lag exerted far more control on the NSE than the damping factor for these periodic signals, and thus we recommend that the damping factor be explicitly considered during calibration.

There are expectedly still some differences between the simulated and observed diurnal signals. In particular, the daily mean of calculated discharge begins to decrease below the daily mean of the measured discharge in the last half of the simulation (Figure 6). Also, on some days the measured discharge lags the simulated discharge, while on other days, the opposite is true. These minor differences could arise do to any of the simplifications associated with the modeling approach, including treating the talus as a prismatic aquifer with constant flow per unit width, spatially averaging the snowmelt flux from UEB for input to SFASH, and ignoring unsaturated zone dynamics (section 4.6). Despite these simplifications, the model structure was able to capture the general damping and lagging dynamics of the output signals (Figure 6).

### 4.6. Limitations

The groundwater flow in the coarse boulder field of the talus unit is complex and difficult to represent in conventional groundwater flow models. The groundwater flow attains velocities that approach or exceed the limit for Darcian flow, and we expect that preferential flow around boulders may be an important

transport mechanism not fully represented in a matrix flow conceptual model. Also, the modeling approach employed herein did not consider the flow dynamics in the unsaturated zone and their role on the timing of the output signal [*Troch et al*., 2013]. As previously noted, we expect that the residence time and signal modulation through the unsaturated zone would be minimal due to the short vertical travel distance compared to the horizontal travel distance as well as the higher hydraulic gradients and preferential flow conduits.

The approach (equation (2)) employed in this study for representing saturated $K$ variation with depth has only been previously used to represent gradual $K$ decrease with depth in organic soils [*Quinton et al*., 2008]. The suitability of this function for representing the sharp transition in $K$ with depth presumed to occur in talus units [*Davinroy*, 2000] warrants further field investigation. In general, the SFASH model, which solves the Boussinesq equation, is a parsimonious modeling approach compared to a three-dimensional numerical model based on Richards equation. Employing a multidimensional numerical model with unsaturated zone physics proved problematic in this study given the steep soil water characteristic curve and the highly nonlinear nature of the governing equations. Readers are directed to *Steenhuis et al*. [1999] and *Paniconi et al*. [2003] for detailed comparisons of models based on the Boussinesq equation to Richards-type numerical models of groundwater flow. Both studies showed that similar outflow hydrographs were generally obtained using either conceptual approach.

The results presented in this study (e.g., Figures 4 and 5) suggest that there may be equifinality issues associated with model calibration from diurnal signals, especially as the number of parameters increases for the heterogeneous cases. Such issues may be potentially limited by considering both the damping and lagging under cyclical hydrologic forcing during melt as well as recession characteristics later in the summer. This deserves further investigation in future studies. Finally, any method to characterize aquifers based on the analysis of diurnal signals is only useful in aquifers that retain such signals. When the driving force for these diurnal signals is caused by surface processes, only thin, shallow aquifers would typically have short residence times, flashy dynamics, and thus retained diurnal signals.

## 5. Summary and Conclusions

Obtaining storage and transmission properties for alpine landforms is a critical step toward understanding their hydrologic functioning and sensitivity to environmental change. Standard, invasive hydrogeological investigation methods are often limited in these harsh, restricted-access environments. Thus naturally occurring diurnal signals provide a unique opportunity for estimating the hydraulic and storage properties of alpine aquifers and hillslopes and for parameterizing hydrological models. In this study, we applied a simple numerical groundwater flow model to simulate the propagation of snowmelt-induced hydraulic pulses. The modeling results provide insight into the various factors that control the damping and lagging of diurnal hydraulic pulses. The simulations indicate that lower $K$ and higher specific yield (i.e., lower hydraulic diffusivity) result in increased damping and lagging. The simulations further illustrate that a low $K$ zone at the base of the aquifer only slightly influences the lagging, but greatly increases the damping. Thus, in the heterogeneous systems considered in this study, the upper higher $K$ layer primarily controlled the lagging, while the thin low $K$ zone primarily controlled the damping.

A cross correlation of the simulated snowmelt signal and the measured stream discharge signal indicated an average lag between the talus input and output of 7 h, and a comparison of the daily amplitudes of the input and output signals via equation (4) revealed an average damping factor of 0.39. Similar results (average lag and damping factor of 7 h and 0.46, respectively) were obtained for SFASH simulations performed with a top saturated $K$ of 0.02 m $s^{-1}$, a 10 cm thick lower $K$ (0.002 m $s^{-1}$) zone, and a specific yield of 0.30. A comparison between the measured and observed discharge in Babylon Creek yielded an NSE of 0.57. Thus the conceptual model and SFASH simulations could be used to reproduce the general characteristics of the observed hydraulic pulse propagation in the talus. This study illustrates the importance of considering both the lagging and damping of the diurnal signals. The hydraulic and storage properties of the aquifer or hillslope influence both characteristics of the signal propagation, and thus considering both may limit equifinality issues with model calibration. The analytical solution considered in this study can only be applied to infer the $K$ from the lag alone, and this approach was shown in this study to result in far too little signal damping for the heterogeneous runs. Thus this solution, which assumes homogeneous conditions, is

limited in terms of its ability to characterize the hydraulic properties of heterogeneous hillslopes and aquifers from diurnal signal lags. Although considerable effort may be required to perform simulations of diurnal signals in a numerical groundwater flow model, only minimal additional effort is required when this process is conducted in models that are already being set up for the aquifer or hillslope in question.

The analyses of diurnal signals to characterize aquifer properties and processes can augment other classic approaches, such as recession analyses. Recession methods typically assume continuous drainage, and this assumption is often violated in the summer months in alpine environments when snow and concomitant recharge persists at higher elevations. Thus, the method proposed in this study is especially applicable for alpine watersheds, which are characterized by subsurface data scarcity and often exhibit diurnal signals due to snow and glacier melt. These naturally occurring diurnal signals are presently underutilized in the hydrological sciences. The analyses of diurnal flow signals to understand hydrological processes was herein demonstrated with a distributed numerical model, but the general method should also be applicable for the parameterization of lumped, distributed, or semidistributed hydrological models. The inferred hydraulic parameters may vary depending on the complexity of the modeling structure employed, but, in each case, those properties would theoretically represent a reasonable parameterization for that modeling structure. Although the present study only considered snowmelt-induced diurnal signals, a similar process could be applied to investigate ET-induced diurnal signals. We anticipate that future studies will apply these techniques in other aquifers and hillslopes with different subsurface environments (e.g., lower $K$) and forcing functions and provide further insight into the uncertainty associated with this parameterization approach.

**Acknowledgments**
Helpful comments from the Associate Editor and two anonymous reviewers are gratefully acknowledged. Jesse He (University of Calgary) is thanked for compiling the UEB model results for the Babylon basin. Data from this study may be obtained from either author. Funding support for the long-term study in the Lake O'Hara watershed was provided by Alberta Ingenuity Centre for Water Research, Environment Canada Science Horizons Program, Biogeoscience Institute (University of Calgary), and Natural Sciences and Engineering Research Council of Canada (NSERC). Logistical support was provided by Lake O'Hara Lodge and Parks Canada. Andrius Paznekas is thanked for his help with the oblique snowpack images. B. Kurylyk was funded via postdoctoral fellowships provided by NSERC, the Killam Trusts, and the University of Calgary Eyes High program.

## References

Bedient, P. B., and W. C. Huber (2002), *Hydrology and Floodplain Analysis*, 289 p., Prentice Hall, Upper Saddle River, N. J.
Bishop, K., J. Seibert, L. Nyberg, and A. Rodhe (2011), Water storage in a till catchment. II: Implications of transmissivity feedback for flow paths and turnover times, *Hydrol. Processes*, *25*, 3950–3959, doi:10.1002/hyp.8355.
Bond, B. J., J. A. Jones, G. Moore, N. Phillips, D. Post, and J. J. McDonnell (2002), The zone of vegetation influence on baseflow revealed by diel patterns of streamflow and vegetation water use in a headwater basin, *Hydrol. Processes*, *16*, 1671–1677, doi:10.1002/hyp.5022.
Boussinesq, J. (1877), Essai sur la théorie des eaux courantes, *Mem. Acad. Sci. Inst. Fr. 23*, 252–260.
Brown, L. E., D. M. Hannah, and A. M. Milner (2007), Vulnerability of alpine stream biodiversity to shrinking glaciers and snowpacks, *Global Change Biol.*, *13*, 958–966, doi:10.1111/j.1365-2486.2007.01341.x.
Brutsaert, W. (1994), The unit response of groundwater outflow from a hillslope, *Water Resour. Res.*, *30*, 2759–2763, doi:10.1029/94WR01396.
Brutsaert, W. (2005), *Hydrology: An Introduction*, Cambridge Univ. Press, Cambridge, U. K.
Caine, N. (1992), Modulation of the diurnal streamflow response by the seasonal snowcover of an alpine basin, *J. Hydrol.*, *137*, 245–260, doi:10.1016/0022-1694(92)90059-5.
Camporese, M., D. Penna, M. Borga, and C. Paniconi (2014), A field and modeling study of nonlinear storage-discharge dynamics for an alpine headwater catchment, *Water Resour. Res.*, *50*, 806–822, doi:10.1002/2013WR013604.
Celia, M. A., E. T. Bouloutas, and R. L. Zarba (1990), A general mass conservative numerical solution for the unsaturated flow equation, *Water Resour. Res.*, *26*, 1483–1496.
Clow, D. W., L. Schrott, R. Webb, D. H. Campbell, A. Torizzo, and M. Dornblaser (2003), Ground water occurrence and contributions to streamflow in an alpine catchment, Colorado Front Range, *Ground Water*, *41*, 937–950, doi:10.1111/j.1745-6584.2003.tb02436.x.
Condom, T., A. Rabatel, M. Villacis, D. Jacobsen, O. Dangles, L. Evolution, C. Cota, and L. Paz (2013), Technical Note: Glacial influence in tropical mountain hydrosystems evidenced by the diurnal cycle in water levels, *Hydrol. Earth Syst. Sci.*, *17*, 4803–4816, doi:10.5194/hess-17-4803-2013.
Crossman, J., C. Bradley, I. Boomer, and A. M. Milner (2011), Water flow dynamics of groundwater-fed streams and their ecological significance in a glacierized catchment, *Arct. Antarct. Alp. Res.*, *43*, 364–379, doi:10.1657/1938-4246-43.3.364.
Davinroy, T. (2000), Hydrologic and biogeochemical characteristics of alpine talus, Colorado Front Range, PhD thesis, University of Colo., Boulder.
DeBeer, C. M., and J. W. Pomeroy (2010), Simulation of the snowmelt runoff contributing area in a small alpine basin, *Hydrol. Earth Syst. Sci.*, *14*, 1205–1219, doi:10.5194/hess-14-1205-2010.
Desjardins, P. R., B. R. Pratt, L. A. Buatois, and M. G. Mángano (2010). Stratigraphy and sedimentary environments of the Lower Cambrian Gog Group in the southern Rocky Mountains of Western Canada: Transgressive sandstones on a broad continental margin, *Bull. Can. Pet. Geol.*, *58*, 403–439, doi:10.2113/gscpgbull.58.4.403.
Deutscher, J., P. Kupec, P. Dundek, L. Holik, M. Machala, and J. Urban (2016), Diurnal dynamics of streamflow in a upland forested micro-watershed during short precipitation-free periods is altered by tree sap flow, *Hydrol. Processes*, *30*, 2042–2049, doi:10.1002/hyp.10771.
Evans, S. G., S. Ge, and S. Liang (2015), Analysis of groundwater flow in mountainous, headwater catchments with permafrost, *Water Resour. Res. 51*, 9564–9576, doi:10.1002/2015WR017732.
Fang, X., J. W. Pomeroy, C. R. Ellis, M. K. Macdonald, C. M. Debeer, and T. Brown (2013), Multi-variable evaluation of hydrological model predictions for a headwater basin in the Canadian Rocky Mountains, *Hydrol. Earth Syst. Sci.*, *17*,1635–1659, doi:10.5194/hess-17-1635-2013.
Fetter, C. W. (2001), *Applied Hydrogeology*, 4th ed., Prentice Hall, Upper Saddle River, N. J.
Graham, C. B., H. R. Barnard, K. L. Kavanagh, and J. P. McNamara (2013.), Catchment scale controls the temporal connection of transpiration and diel fluctuations in streamflow, *Hydrol. Processes*, *27*, 2541–2556, doi:10.1002/hyp.9334.
Gribovszki, Z., J. Szilágyi, and P. Kalicz (2010), Diurnal fluctuations in shallow groundwater levels and streamflow rates and their interpretation: A review, *J. Hydrol.*, *385*, 371–383, doi:10.1016/j.jhydrol.2010.02.001.
Hood, J. L., and M. Hayashi (2015), Characterization of snowmelt flux and groundwater storage in an alpine headwater basin, *J. Hydrol.*, *521*, 482–497, doi:10.1016/j.jhydrol.2014.12.041.

Hood, J. L., J. W. Roy, and M. Hayashi (2006), Importance of groundwater in the water balance of an alpine headwater lake, *Geophys. Res. Lett. 33*, L13405, doi:10.1029/2006GL026611.
Kaser, G., M. Großhauser, and B. Marzeion (2010), Contribution potential of glaciers to water availability in different climate regimes, *Proc. Nat. Acad. Sci. U. S. A.*, *107*, 20,223–20,227, doi:10.1073/pnas.1008162107.
Langston, G., L. R. Bentley, M. Hayashi, A. McClymont, and A. Pidlisecky (2011), Internal structure and hydrological functions of an alpine proglacial moraine, *Hydrol. Processes*, *25*, 2967–2982, doi:10.1002/hyp.8144.
Lickorish, W. H., and P. S. Simony (1995), Evidence for late rifting of the Cordilleran margin outlined by stratigraphic division of the Lower Cambrian Gog Group, Rocky Mountain Main Ranges, British Columbia and Alberta, *Can. J. Earth Sci.*, *32*, 860–874, doi:10.1139/e95-072.
Loheide, S.P. and J.D. Lundquist (2009), Snowmelt-induced diel fluxes through the hyporheic zone, *Water Resour. Res.*, *45*, W07404, doi: 10.1029/2008WR007329.
Lowry, C. S., J. S. Deems, S. P. Loheide, and J. D. Lundquist (2010), Linking snowmelt-derived fluxes and groundwater flow in a high elevation meadow system, Sierra Nevada Mountains, California, *Hydrol. Processes*, *24*, 2821–2833, doi:10.1002/hyp.7714.
Lundquist, J. D., and D. R. Cayan (2002), Seasonal and spatial patterns in diurnal cycles in streamflow in the western United States, *J. Hydrometeorol.*, *3*, 591–603, doi:10.1175/1525-7541(2002)003 < 0591:SASPID>2.0.CO;2.
Magnusson, J., F. Kobierska, S. Huxol, M. Hayashi, T. Jonas, and J.W. Kirchner (2014), Melt water driven stream and groundwater stage fluctuations on a glacier forefield (Dammagletscher, Switzerland), *Hydrol. Processes*, *28*, 823–836, doi:10.1002/hyp.9633.
Markovich, K. H., R. M. Maxwell, and G. E. Fogg (2016), Hydrogeological response to climate change in alpine hillslopes, *Hydrol. Processes*, *30*, 3126–3138, doi:10.1002/hyp.10851.
Marks, D., and J. Dozier (1992), Climate and energy exchange at the snow surface in the Alpine Region of the Sierra Nevada: 2. Snow cover energy balance, *Water Resour. Res. 18*, 3043–3054, doi:10.1029/92WR01483.
Marks, D., J. Domingo, D. Susong, T. Link, and D. Garen (1999), A spatially distributed energy balance snowmelt model for application in mountain basins, *Hydrol. Processes*, *13*, 1935–1959, doi:10.1002/(SICI)1099-1085(199909)13:12/13 < 1935::AID-HYP868 > 3.0.CO;2-C.
Marsh, P., and J. W. Pomeroy (1996), Meltwater fluxes at an arctic forest-tundra site, *Hydrol. Processes*, *10*, 1383–1400, doi:10.1002/(SICI)1099-1085(199610)10:10 < 1383::AID-HYP468 > 3.0.CO;2-W.
Marsh, P., and M.-K. Woo (1984), Wetting front advance and freezing of meltwater within a snow cover: 1 Observations in the Canadian Arctic, *Water Resour. Res.*, *20*, 1853–1864, doi:10.1029/WR020i012p01853.
McClymont, A.F., M. Hayashi, M., LR. Bentley, D. Muir, and E. Ernst (2010), Groundwater flow and storage within an alpine meadow-talus complex, *Hydrol. Earth Syst. Sci.*, *14*, 859–872, doi:10.5194/hess-14-859-2010.
Mendoza, G. F., T. S. Steenhuis, M. T. Walter, and J. Parlange (2003), Estimating basin-wide hydraulic parameters of a semi-arid mountainous watershed by recession-flow analysis, *J. Hydrol.*, *279*, 57–69, doi:10.1016/S0022-1694(03)00174-4.
Muir, D. L., M. Hayashi, and A. F. McClymont (2011), Hydrological storage and transmission characteristics of an alpine talus, *Hydrol. Processes*, *25*, 2954–2966, doi:10.1002/hyp.8060.
Mutzner, R., S. V. Weijs, P. Tarolli, M. Calaf, H. J. Oldroyd, and M. B. Parlange (2015), Controls on the diurnal streamflow cycles in two subbasins of an alpine headwater catchment, *Water Resour. Res. 51*, 3403–3418, doi:10.1002/2014WR016581.
Nash, J. E. and J. V. Sutcliffe (1970), River flow forecasting through conceptual models part I -A discussion of principles, *J. Hydrol.*, *10*(3), 282–290.
Paniconi, C., P. A. Troch, E. E. van Loon, and A. G. J. Hilberts (2003), Hillslope-storage Boussinesq model for subsurface flow and variable source areas along complex hillslopes: 2. Intercomparison wih a three-dimensional Richards equation model, *Water Resour. Res. 39*(11), 1317, doi:10.1029/2002WR001730.
Pauritsch, M., S. Birk, T. Wagner, S. Hegarten, and G. Winkler (2015), Analytical approximations of discharge recessions for steeply sloping aquifers in alpine catchments, *Water Resour. Res. 51*, 8729–8740, doi:10.1002/2015WR017749.
Pepin, N., et al. [Mountain Research Initiative EDW Working Group] (2015), Elevation-dependent warming in mountain regions of the world, *Nat. Clim. Change 5*, 424–430, doi:10.1038/nclimate2563.
Pomeroy, J. W., D. M. Gray, K. R. Shook, B. Toth, R. L. H. Essery, A. Pietroniro, and N. Hedstrom (1998), *Hydrol. Processes*, *12*, 2339–2367, doi: 10.1002/(SICI)1099-1085(199812)12:15 < 2339::AID-HYP800 > 3.0.CO;2-L.
Quinton, W. L., M. Hayashi, and S. K. Carey (2008), Peat hydraulic conductivity in cold regions and its relation to pore size and geometry, *Hydrol. Processes*, *22*, 2829–2837, doi:10.1002/hyp.7027.
Rasouli, K., J. W. Pomeroy, J. R. Janowicz, S. K. Carey, and T. J. Williams (2014), Hydrological sensitivity of a northern mountain basin to climate change, *Hydrol. Processes*, *28*, 4191–4208, doi:10.1002/hyp.10244.
R Core Team (2014), *R: A Language and Environment for Statistical Computing*. R Found. for Stat. Comput., Vienna, Austria. [Available at http://www.R-project.org/.]
Rupp, D. E., and J. S. Selker (2006a), On the use of the Boussinesq equation for interpreting recession hydrographs from sloping aquifers, *Water Resour. Res.*, *42*, W12421, doi:10.1029/2006WR005080.
Rupp, D. E., and J. S. Selker (2006b), Information, artifacts, and noise in dQ/dt -Q recession analysis, *Adv. Water Res.*, *29*, 154–160, doi: 10.1016/j.advwatres.2005.03.019.
Spence, C., and M-k. Woo (2003), Hydrology of subarctic Canadian shield: Soil-filled valleys, *J. Hydrol.*, *279*, 1–4, doi:10.1016/S0022-1694(03)00175-6.
Steenhuis, T. S., J.-Y. Parlange, W. E. Stanford, A. Heilig, F. Stagnitti, and M. F. Walter (1999), Can we distinguish Richards' and Boussinesq's equations for hillslopes?: The Coweeta experiment, *Water Resour. Res,. 35*, 589–593, doi:10.1029/1998WR900067.
Tague, C. and G.E. Grant (2009), Groundwater dynamics mediate low-flow response to global warming in snow-dominated alpine regions, *Water Resour. Res.*, *45*, W07421, doi:10.1029/2008WR007179.
Tarboton, D. G., and C. H. Luce (1996), *Utah Energy Balance Snow Accumulation and Melt Model (UEB): Computer Model Technical Description and Users Guide*, Utah Water Res. Lab., Logan, Utah.
Tarboton, D. G., T. G. Chowdhury, and T. H. Jackson (1995), A spatially distributed energy balance snowmelt model, in *Biogeochemistry of Snow Cover Catchments*, *IAHS Publ.*, *228*, pp. 141–155.
Troch, P. A., et al. (2013), The importance of hydraulic groundwater theory in catchment hydrology: The legacy of Wilfried Brutsaert and Jean-Yves Parlange, *Water Resour. Res. 49*, 5099–5116, doi:10.1002/wrcr.20407.
Tromp-van Meerveld, H. J., and J. J. McDonnell (2006), Threshold relations in subsurface stormflow: 2. The fill and spill hypothesis, *Water Resour. Res.*, *42*, W02411, doi:10.1029/2004WR003800.
Viviroli, D., H. H. Dürr, B. Messerli, M. Meybeck, and R. Weingartner (2007), Mountains of the world, water towers for humanity: Typology, mapping, and global significance, *Water Resour. Res. 43*, W07447, doi:10.1029/2006WR005653.

Viviroli, D., D. R. Archer, W. Buytaert, H. J. Fowler, G. B. Greenwood, A. F. Hamlet, and Y. Huang (2011), Climate change and mountain water resources: Overview and recommendations for research, management and policy, *Hydrol. Earth Syst. Sci.*, *15*, 471–504, doi:10.5194/hess-15-471-2011.

Wigmosta, M. S., and D. P. Lettenmaier (1999), A comparison of simplified methods for routing topographically driven subsurface flow, *Water Resour. Res.*, *35*, 255–264.

Wright, N., M. Hayashi, and W. L. Quinton (2009), Spatial and temporal variations in active layer thawing and their imiplication on runoff generation in peat-covered permafrost terrain, *Water Resour. Res.*, *45*, W05414, doi:10.1029/2008WR006880.

Zierl, B., and H. Hugmann (2005), Global change impacts on hydrological processes in Alpine catchments, *Water Resour. Res. 41*, W02028, doi:10.1029/2004WR003447.